NASA TECHNICAL NOTE

NASA TN D-2000

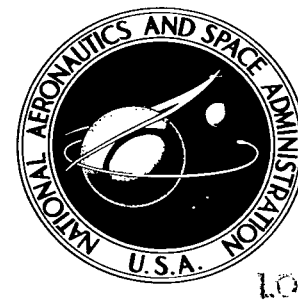

NASA TN D-2000

HEAT-TRANSFER AND PRESSURE MEASUREMENTS ON A PRELIMINARY PROJECT FIRE MODEL AT MACH 3.51

by Robert L. Stallings, Jr., and Kenneth V. Haggard

Langley Research Center
Langley Station, Hampton, Va.

NATIONAL AERONAUTICS AND SPACE ADMINISTRATION • WASHINGTON, D. C. • NOVEMBER 1964

HEAT-TRANSFER AND PRESSURE MEASUREMENTS ON A PRELIMINARY PROJECT FIRE MODEL AT MACH 3.51

By Robert L. Stallings, Jr., and Kenneth V. Haggard

Langley Research Center
Langley Station, Hampton, Va.

NATIONAL AERONAUTICS AND SPACE ADMINISTRATION

For sale by the Office of Technical Services, Department of Commerce,
Washington, D.C. 20230 -- Price $0.75

HEAT-TRANSFER AND PRESSURE MEASUREMENTS ON A PRELIMINARY PROJECT FIRE MODEL AT MACH 3.51

By Robert L. Stallings, Jr., and Kenneth V. Haggard
Langley Research Center

SUMMARY

Heat-transfer and pressure measurements have been obtained on a preliminary Project Fire model through an angle-of-attack range from 0° to $\pm 10^\circ$ at a Reynolds number of 3.6×10^6 and a Mach number of 3.51. Heat-transfer measurements were also obtained at a Reynolds number of 2.1×10^6. Both heat-transfer and pressure measurements were obtained at the higher Reynolds number with probe-type protuberances simulating external antennas installed on the basic model.

The pressure measurements obtained on the basic configuration are overpredicted by the Newtonian theory in the nose-shoulder corner region at an angle of attack of zero degrees. Pressure measurements and schlieren photographs indicate separated flow on the model afterbody throughout the range of test variables. Elevated pressures were obtained in the interference regions created by the probe protuberances when located 0.75 inch from the model-shoulder surface. The effects of the probes on the model pressure distribution appeared to be confined to the nose-shoulder region in the vicinity of the probe installation. Increasing the distance between the probe and model surface to 1.5 inches resulted in a large decrease in the interference effects on the pressure distribution.

Measured heat-transfer-coefficient distributions on the model nose at zero degrees angle of attack were in fair agreement with existing simplified theories at both Reynolds numbers. Increasing angle of attack resulted in an increase in heating on the windward side of the model nose and a decrease on the leeward side; the maximum value occurred on the windward side at the point of tangency of the nose and corner radii throughout the angle-of-attack range. Large increases in heating were obtained in the probe interference regions; the maximum increase, some 400 percent, was obtained with the probe located 0.75 inch from the model surface.

INTRODUCTION

One of the major problem areas associated with a planetary or lunar mission consists of the severe aerodynamic heating the spacecraft will encounter

during the reentry phase of the mission. The quantitative treatment of this problem is difficult because of the lack of ground facilities capable of simulating such an environment. In order to minimize the hazards associated with this problem area, the Project Fire Program was initiated at the NASA Langley Research Center with the objective of measuring in flight the aerodynamic heating for an environment created by a reentry speed of 37,000 feet per second. The information will be obtained by launching an instrumented payload with a multistage booster on a ballistic trajectory; the first stage will be used to obtain the desired altitude and the downward firing will be used to obtain the desired attitude and velocity at reentry.

In order to supplement the design of the Project Fire payload, heat-transfer and pressure distributions were obtained on a model representing a preliminary Project Fire design in the Langley Unitary Plan wind tunnel. Tests were also conducted with two series of probes simulating external antennas attached to the basic model.

The investigation was conducted at Mach 3.51, angles of attack from -10° to $+10^{\circ}$, and Reynolds numbers per foot of 3.6×10^{6} and 2.1×10^{6}.

SYMBOLS

c	specific heat of model skin, Btu/lb-$^{\circ}$R
c_p	specific heat of air at constant pressure, Btu/slug-$^{\circ}$R
C_p	pressure coefficient, $\left(p_l - p_\infty\right)/q_\infty$
$C_{p,max}$	pressure coefficient corresponding to stagnation pressure behind normal shock
D	model nose diameter, ft
h	heat-transfer coefficient, Btu/sec-sq ft-$^{\circ}$R
k	thermal conductivity of air, Btu/sec-ft-$^{\circ}$R
M	free-stream Mach number
o,n	limits of integration, sec
p	pressure, lb/sq ft
N_{Pr}	Prandtl number, 0.72
q_∞	free-stream dynamic pressure, lb/sq ft
r_o	radius of model cross section, ft

R	free-stream Reynolds number per foot, $\rho_\infty v_\infty/\mu_\infty$
s	surface length measured from center of model nose, ft
s'	surface length from center of model nose to point of tangency of nose and corner radii, 0.372 ft
t	time, sec
T	temperature, $^\circ R$
$T_{w,e}$	measured wall temperature at steady-state conditions, $^\circ R$
$T_{w,n}$	wall temperature at completion of integration, $^\circ R$
$T_{w,o}$	wall temperature at beginning of integration, $^\circ R$
v	velocity, ft/sec
w	weight per unit area of model skin, lb/sq ft
α	angle of attack, deg
θ	polar angle for identification of instrumentation location (see fig. 2(a)), deg
ϕ	angle between free-stream-velocity vector and a normal to model surface, deg
ρ	density of air, slugs/cu ft
μ	viscosity of air, slugs/ft-sec
δ	distance from model surface to probe, in.

Subscripts:

w	conditions at model wall
t	stagnation
$t,2$	stagnation conditions behind normal shock
l	local conditions at outer edge of boundary layer
∞	free stream

APPARATUS, MODELS, AND INSTRUMENTATION

Apparatus

The present investigation was conducted in the high Mach number test section of the Langley Unitary Plan wind tunnel described in reference 1. This variable-pressure continuous-flow tunnel has an asymmetrical sliding-block nozzle that permits continuous operation through a range of Mach numbers from 2.3 to 4.65. The deviation in Mach number over the entire 4- by 4-foot test section for a Mach number of 3.51 is ± 0.05.

Models and Instrumentation

The basic model installed in the wind tunnel is shown in figure 1 and the pertinent dimensions and instrumentation locations are shown in figure 2. The model is described by a 14.69-inch nose radius with a 0.96-inch corner radius which fairs into a cylindrical shoulder section. The afterbody consists of a rearward-facing 33° semiapex conical section. The model was spun in two sections (nose cap and afterbody) from 0.030-inch inconel sheet; the nominal skin thickness was maintained to within ± 0.001 inch. All supporting bulkheads inside the model were constructed from a low thermal-conductivity insulation material and were relieved in the vicinity of the thermocouple installations to minimize conduction losses. The interior of the model was vented to base pressure in order to minimize internal convection. The thermocouple instrumentation consisted of 40 number 30 gage iron-constantan thermocouples spotwelded to the inner surface of the model skin. The pressure instrumentation consisted of thirty-nine 0.050-inch inside-diameter pressure orifices.

Figure 2(b) shows two types of probe protuberances tested and the installation of the probes on the basic configuration. The probes were cylindrical in shape and capped by (1) a hemispherically blunted nose and (2) a sharp 10° conical nose. The protuberances were machined from stainless steel and were attached to the model afterbody immediately aft of the nose shoulder. Both types of probes were tested in pairs at distances of 1.5 inches and 0.75 inch from the model-shoulder surface.

DATA RECORDING, DATA REDUCTION, AND ACCURACY

Data Recording

The thermocouple outputs were amplified, digitized, and magnetically recorded on a high-speed analog-to-digital recording system. Although this system can sample at rates up to 40 times a second, the thermocouple outputs for this test were recorded only every 1/2 second.

The model pressures were measured with a multichannel electrical transducer, the output of which was digitized on a self-balancing potentiometer and

recorded on punch cards. The tunnel free-stream static and stagnation pressures were measured on precision mercury manometers.

Method of Heat-Transfer Data Reduction

The heat-transfer coefficients were obtained from transient skin-temperature measurements resulting from a stepwise increase in tunnel stagnation temperature as discussed in reference 2 by utilizing the following equation:

$$h = \frac{wc\frac{dT_w}{dt}}{T_{w,e} - T_w} \tag{1}$$

This simplified form of the heat-balance equation is obtained by assuming constant temperature through the model skin, negligible lateral heat flow, negligible heat flow to the model interior, and no losses due to radiation. The magnitude of the lateral heat flow was estimated by using temperature measurements of adjacent thermocouples and was found to be negligible. The heat exchange by radiation is dependent upon the term $\sigma\left(T_w^4 - T_a^4\right)$ where T_a is the tunnel wall temperature and σ is the Stephan-Boltzmann constant. This radiated heat flux is very small compared with the heat flux convected into the model skin.

Equation (1) can be rewritten in the following integral form which is suitable for complete machine calculations:

$$h = \frac{wc\left(T_{w,n} - T_{w,o}\right)}{\frac{T_{w,e}}{T_t}\int_0^n T_t\,dt - \int_0^n T_w\,dt} \tag{2}$$

The integrals are evaluated over increments of 1/2 second according to the trapezoidal rule as follows:

$$\int_0^n T\,dt = \Delta t\left(\tfrac{1}{2}T_o + \tfrac{1}{2}T_n + T_1 + T_2 + \ldots + T_{n-1}\right) \tag{3}$$

The ratio $T_{w,e}/T_t$ is experimentally measured prior to the temperature step and is assumed to be invariant with time.

Accuracy

An estimation of the accuracy of the heat-transfer measurements in the Langley Unitary Plan wind tunnel has been indicated by the repeatability of data in tests discussed in reference 3. The accuracy is dependent upon the magnitude

of the heat-transfer coefficient. For $h > 0.0150$, the accuracy is within 10 percent; for $0.001 < h < 0.0150$ within 15 percent; and for $h < 0.0010$, within 20 percent. Although $h < 0.0010$ is within the accuracy of the data, no significance is attached to relative magnitudes in this region other than to indicate the low heat-transfer regions.

The accuracy of the precision manometers is within 0.5 lb/sq ft; therefore, the accuracy of the pressure recording system is governed by that of the electrical transducer which is 0.1 percent of full-scale deflection. The error in the pressure coefficient resulting from this inaccuracy could be ± 0.015.

RESULTS AND DISCUSSION

Schlieren photographs of the model are presented in figure 3(a) for the angle-of-attack range at $R = 3.6 \times 10^6$. Shown in figure 3(a) is the basic configuration; figure 3(b) shows the basic configuration with blunt probe extended 0.75 inch; and, figure 3(c) shows the basic configuration with the sharp probe extended 0.75 inch. It should be noted that throughout the range of variables shown the presence of the white line or slipstream on the schlieren photographs emanating from the corner of the nose cap and afterbody juncture indicates the flow remained separated over the afterbody. The location of the flow reattachment and the resulting shock wave formation is located downstream of the model base on the model sting.

As shown in figure 2(a), the thermocouples and pressure orifices were located in opposite quadrants of the model, and thus in order to obtain complete heat-transfer and pressure distributions, it was necessary to conduct tests at both positive and negative angles of attack. At positive and negative angles of attack, the quadrant containing the thermocouples is windward and leeward, respectively, whereas the pressure instrumentation is, respectively, leeward and windward, $\theta = 0^\circ$ or 180° being in the plane of the angle of attack. In order to simplify the discussion herein when discussing data at the positive or negative angles of attack they will simply be referred to as windward or leeward.

Pressure-Coefficient Distributions

Basic model.- Measured pressure-coefficient distributions obtained on the basic model with and without the probe protuberances are presented in figure 4 through the angle-of-attack range of the tests. A modified Newtonian distribution determined from the following equation is also presented for comparison purposes at zero degrees angle of attack:

$$C_p = C_{p,max} \cos^2 \phi \tag{4}$$

The pressure coefficient $C_{p,max}$ is based on the stagnation pressure behind a normal shock at the free-stream Mach number, and ϕ is the angle between the free-stream velocity vector and local normal to the model surface.

The disagreement of the Newtonian and measured pressure distributions on the basic configuration as shown in figure 4(a) is similar to that generally associated with a blunted nose shape consisting of a hemispherical segment, the segment being terminated prior to the location of the sonic point on a true hemisphere. Increasing angle of attack resulted in an increase in the measured pressure coefficients on the windward side of the nose cap and a decrease on the leeward side. This effect is most predominate in the plane of α ($\theta = 0^{\circ}$) and is insignificant at $\theta = 90^{\circ}$ as would be expected. The C_p distributions on the afterbody ($s/s' > 1.44$) are invariant throughout the angle-of-attack range of the tests; this apparently is due to the occurrence of flow separation as indicated by the schlieren photographs.

Probe effects.- The effect of the probes located at distances of 0.75 inch and 1.5 inches from the model surface are presented in figure 4(b). Since the probe effects on the pressure measurements throughout the range of test variables were confined to the instrumentation located on the nose cap in the vertical plane of symmetry, only these data are presented. In general, the probe effects of either probe consist of an increase in the pressure coefficients in the immediate vicinity of the probe installation, the magnitude of which decreases with increasing the distance from the probe to the model surfaces.

Heat Transfer

Basic model.- The measured heat-transfer-coefficient distributions are presented in figure 5 throughout the range of α at $R = 3.6 \times 10^6$. A theoretical distribution is also presented on the figure for zero degrees angle of attack determined by the method of reference 4 for $s/s' > 0$ and by the method of reference 5 for the stagnation point, $s/s' = 0$. Although there are more refined theories available which have shown better agreement with experimental data, these theories generally require a much more detailed pressure distribution than obtained in these tests. The stagnation-point solution of reference 4 was rearranged to include free-stream conditions and resulted in the following expression.

$$h\sqrt{D} = 0.662 k_w \left(\frac{dv}{ds} \frac{D}{v_\infty} R \frac{\mu_\infty}{\mu_w} \frac{p_{t,2}}{p_\infty} \frac{T_\infty}{T_w} \right)^{1/2} \qquad (5)$$

The parameter $\frac{dv}{ds} \frac{D}{v_\infty}$ could not be determined from the experimental pressure data as a result of the lack of detailed pressure instrumentation in the stagnation-point region. The parameter was assumed to correspond to that for a hemisphere and was determined from the data of reference 6.

The theoretical distribution for $s/s' > 0$ was determined from the following equation from reference 4 which was simplified by assuming constant specific heat

$$h = 0.47 N_{Pr}^{-2/3} \frac{c_p \rho_l \mu_l v_l r_o}{\left(2 \int_0^s \rho_l \mu_l v_l r_o^2 ds\right)^{1/2}} \tag{6}$$

The local conditions indicated in equation (6) were determined from local pressures obtained by fairing a smooth curve through the measured pressures and by assuming an isentropic expansion from the forward stagnation point.

The experimental heating rates on the front face of the basic model at $\alpha = 0^o$ figure 5(a) are in fair agreement with theory except in the vicinity of $s/s' = 1$ where experiment shows a slight increase in heating that is not indicated by theory. Although the magnitude of this increase is within the accuracy of the data, it persistently occurs in the distribution at all three values of θ. It is within this region that a peak value and large gradients occur in the term $\rho_l \mu_l v_l r_o$ of equation (6) requiring extremely accurate and detailed pressure distributions. Application of the theory of reference 4 in this region is also questionable because of its derivation being based on the assumption of small pressure gradients. For $s/s' > 1$, theory and experiment are generally in very good agreement. The heating rates obtained on the afterbody in a region of flow separation for zero degrees angle of attack are approximately of the same magnitude as those obtained on the shoulder at $s/s' = 1.38$; however, a comparison of the relative magnitudes in the regions of low heating is considered unreliable because of potentially large errors in the measurements.

Increasing angle of attack resulted in the anticipated increase in heating on the windward side of the nose cap and a decrease on the leeward side; the largest effects occurred in the plane of α ($\theta = 180^o$). Throughout the range of α the maximum heating rate occurred at $s/s' = 1$ on the windward face. At $\alpha = 10^o$, this peak heating rate for $\theta = 180^o$ is approximately 25 percent greater than the value obtained at the same location for $\alpha = 0^o$ and approximately 40 percent greater than the zero angle-of-attack stagnation-point value. There was no apparent increase on the windward afterbody heating rates throughout the range of α.

Probe effects.- The effects of the probes on the nose-cap heating distribution for values of $\delta = 0.75$ and 1.5 inches are presented in figure 5(b). Similar to the results obtained for the pressure distribution, the probe effects on the heating distribution were confined to the vertical plane of symmetry of the nose cap and, therefore, only those data are presented. In general, the probe effects consist of an increase in heating initially occurring on the model shoulder. The maximum increase compared with the values for the basic model in figure 5(a) was approximately 400 percent and occurred in the interference region created by the blunt probe located 0.75 inch from the model surface at $\alpha = 0^o$. It should be noted that part of the probe effects shown could be

associated with boundary-layer transition resulting from the flow instability and adverse pressure gradients created by the probes. Due to the relatively small region on the model influenced by the probes, an assessment of the extent of the effects of transition, if present, cannot be obtained.

Heating distributions obtained on the basic configuration through the range of angle of attack at $R = 2.10 \times 10^6$ are presented in figure 6. There is no discernible effect of decreasing Reynolds number on the heating distributions other than a general decrease in the magnitude of the heating rates. The experimental data at $\alpha = 0^\circ$ is in fair agreement with the theoretical distribution of reference 4.

CONCLUDING REMARKS

Heat-transfer and pressure measurements obtained on a preliminary Project Fire model through a range of angles of attack from 0° to $\pm 10^\circ$ and Reynolds numbers of 2.1×10^6 and 3.6×10^6 at Mach 3.51 indicate the following:

1. Pressure measurements obtained on the basic configuration are overpredicted by Newtonian theory in the nose-shoulder corner region at zero degrees angle of attack.

2. Pressure measurements and schlieren photographs indicated separated flow on the afterbody throughout the range of test variables.

3. Elevated pressure coefficients were obtained in interference regions created by probes simulating external antennas when located 0.75 inch from the shoulder of the basic model. This effect was apparent only on the nose-shoulder region in the vicinity of the protuberance installation. Increasing the distance between the probe and model surface to 1.5 inches resulted in a large decrease in the effects of the interference region on the pressure distributions.

4. Measured heat-transfer coefficients on the model nose at zero degrees angle of attack were in fair agreement with values obtained from existing simplified theories at both Reynolds numbers. Increasing angle of attack resulted in an increase in heating on the windward side of the nose cap and a decrease on the leeward side; the maximum value occurred on the windward side at the point of tangency of the nose and corner radii throughout the angle-of-attack range.

5. Large increases in heating were obtained in the probe interference regions; the maximum increase, some 400 percent, was obtained with the probe located 0.75 inch from the model surface.

Langley Research Center,
National Aeronautics and Space Administration,
Langley Station, Hampton, Va., June 5, 1964.

REFERENCES

1. Anon.: Manual for Users of the Unitary Plan Wind Tunnel Facilities of the National Advisory Committee for Aeronautics. NACA, 1956.

2. Burbank, Paige B., and Hodge, B. Leon: Distribution of Heat Transfer on a 10° Cone at Angles of Attack From 0° to 15° for Mach Numbers of 2.49 to 4.65 and a Solution to the Heat-Transfer Equation That Permits Complete Machine Calculations. NASA MEMO 6-4-59L, 1959.

3. Taylor, Nancy L., Hodge, Ward F., and Burbank, Paige B.: Heat-Transfer and Pressure Measurements of a 1/7-Scale Model of a Mercury Capsule at Angles of Attack From 0° to ±20° at Mach Numbers of 3.50 and 4.44. NASA TM X-522, 1961.

4. Vaglio-Laurin, Roberto: Laminar Heat Transfer on Three-Dimensional Blunt Nosed Bodies in Hypersonic Flow. ARS Jour., vol. 29, no. 2, Feb. 1959, pp. 123-129.

5. Sibulkin, M.: Heat Transfer Near the Forward Stagnation Point of a Body of Revolution. Jour. Aero. Sci. (Readers' Forum), vol. 19, no. 8, Aug. 1952, pp. 570-571.

6. Korobkin, Irving: Laminar Heat Transfer Characteristics of a Hemisphere for the Mach Number Range 1.9 to 4.9. NAVORD Rep. 3841 (Aeroballistic Res. Rep. 257), U.S. Naval Ord. Lab. (White Oak, Md.), Oct. 10, 1954.

Figure 1.- Installation of model in test section. L-62-6258

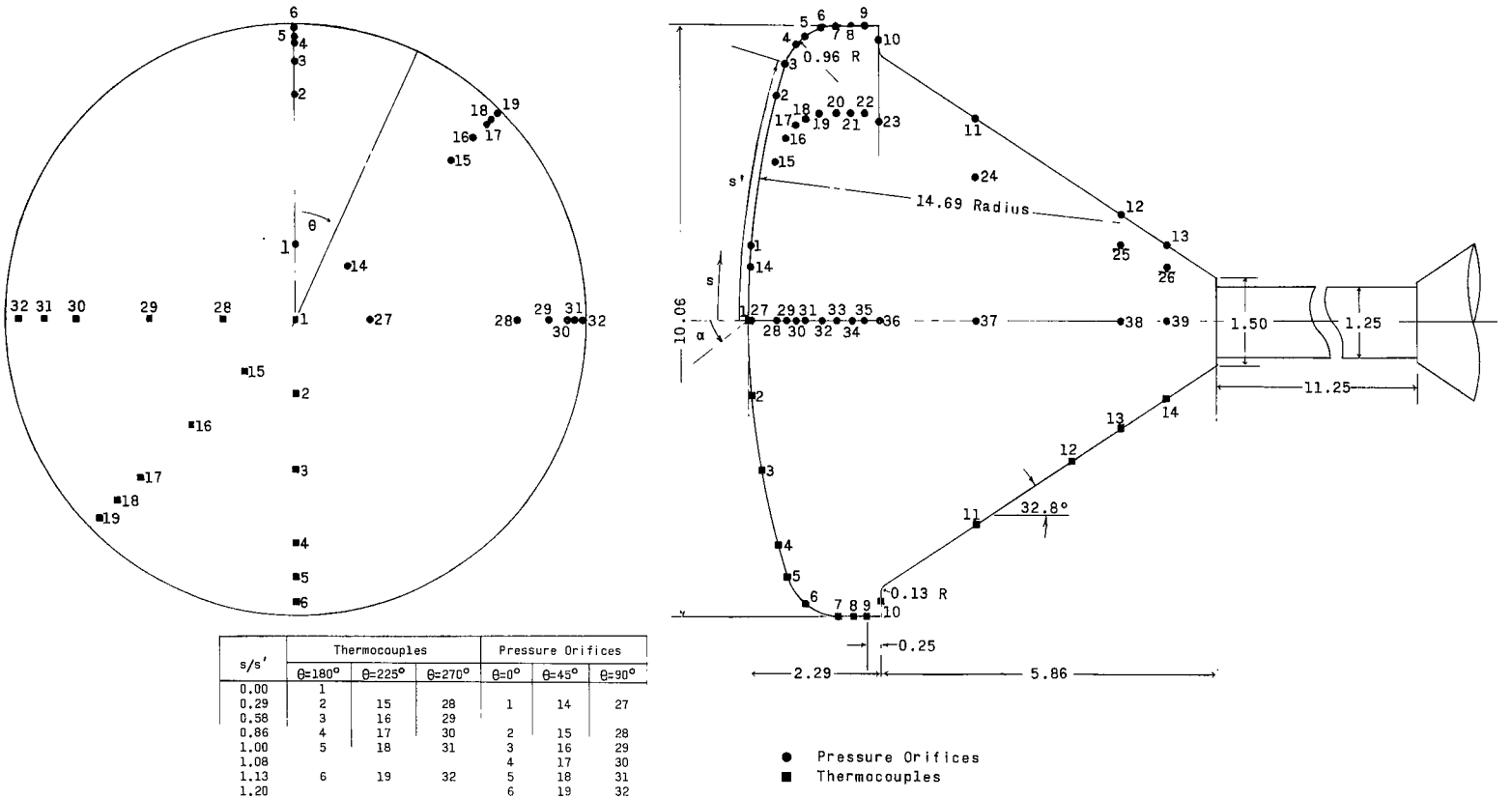

s/s'	Thermocouples			Pressure Orifices		
	θ=180°	θ=225°	θ=270°	θ=0°	θ=45°	θ=90°
0.00	1					
0.29	2	15	28	1	14	27
0.58	3	16	29			
0.86	4	17	30	2	15	28
1.00	5	18	31	3	16	29
1.08				4	17	30
1.13	6	19	32	5	18	31
1.20				6	19	32
1.26	7	20	33	7	20	33
1.32	8	21	34	8	21	34
1.38	9	22	35	9	22	35
1.48	10	23	36	10	23	36
1.97	11	24	37	11	24	37
2.42	12	25	38	12	25	38
2.65	13	26	39			
2.87	14	27	40	13	26	39

(a) Instrumentation location.

Figure 2.- Model drawings. (All dimensions in inches.)

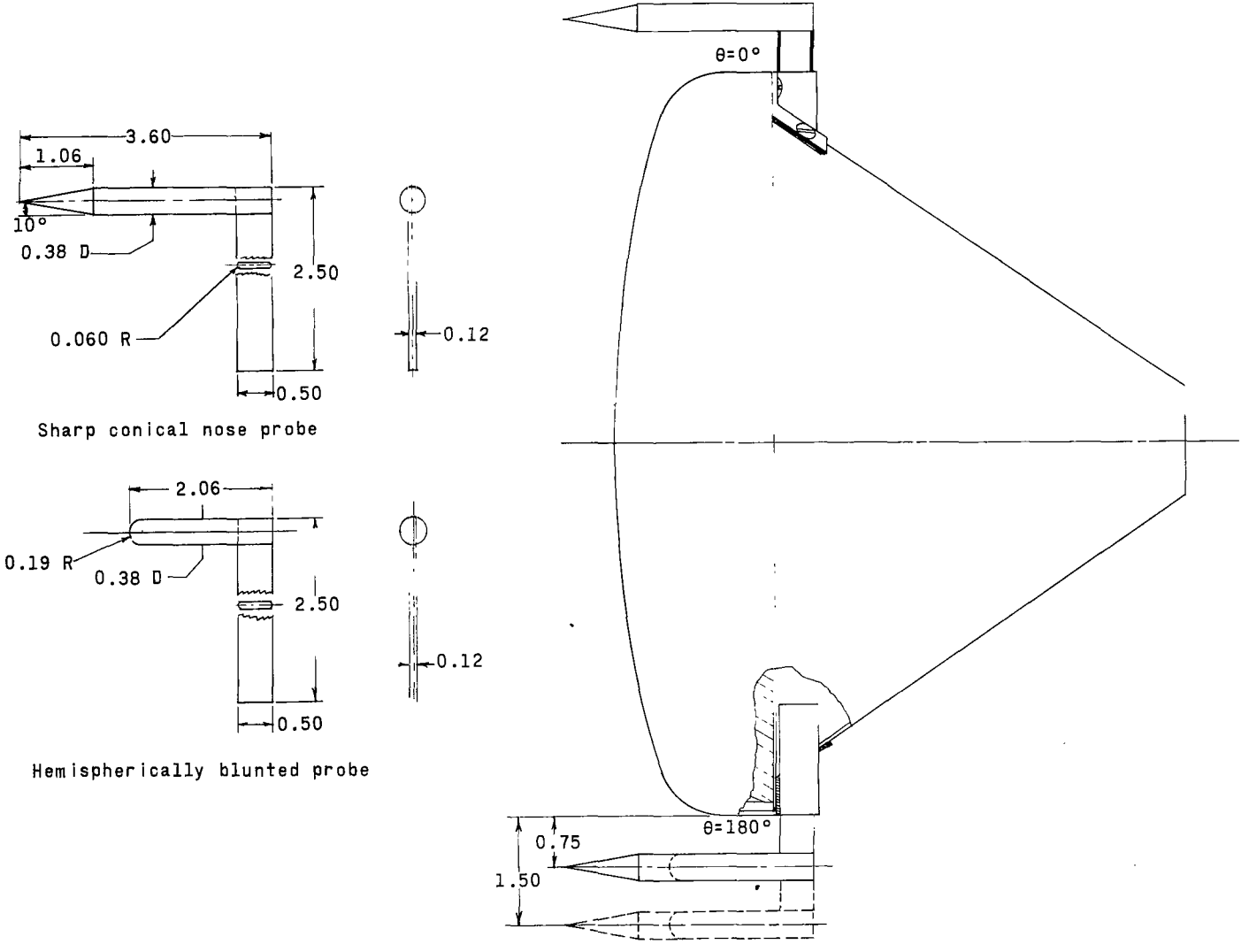

(b) Description and installation of probe protuberances to basic model.

Figure 2.- Concluded.

$\alpha = 0°$

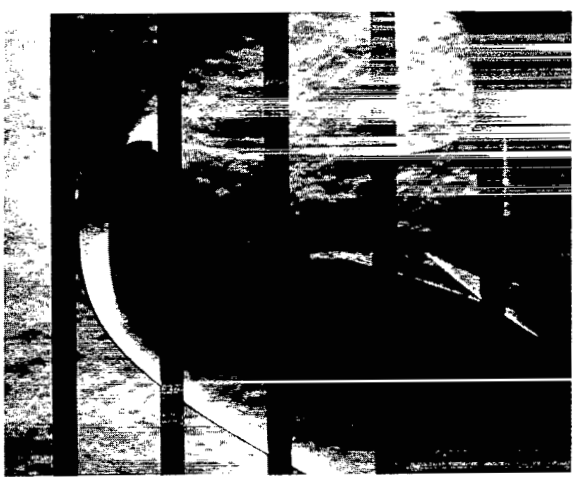

$\alpha = 5°$

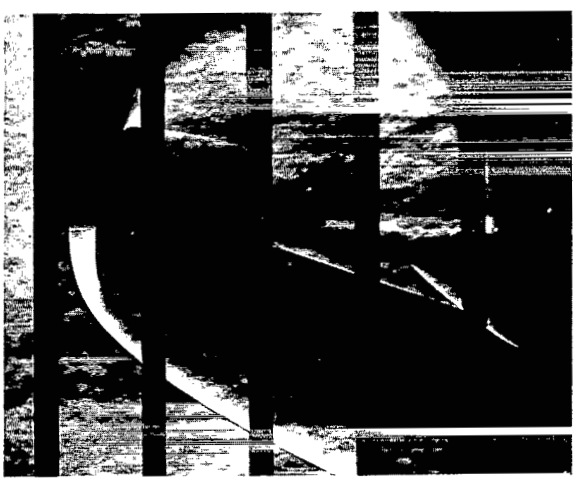

$\alpha = 10°$

(a) Basic configuration.

L-64-4709

Figure 3.- Schlieren photographs; M = 3.51; R = 3.60×10^6.

$\alpha = 0°$

$\alpha = 10°$

L-64-4710

(b) Basic configuration with blunt probe extended 0.75 inch.

Figure 3.- Continued.

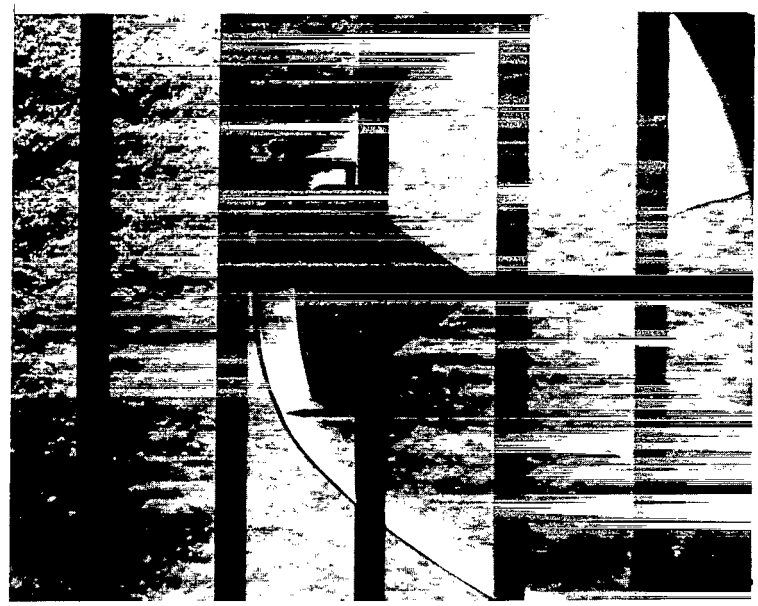

$\alpha = 0°$

$\alpha = 10°$

L-64-4711

(c) Basic configuration with sharp probe extended 0.75 inch.

Figure 3.- Concluded.

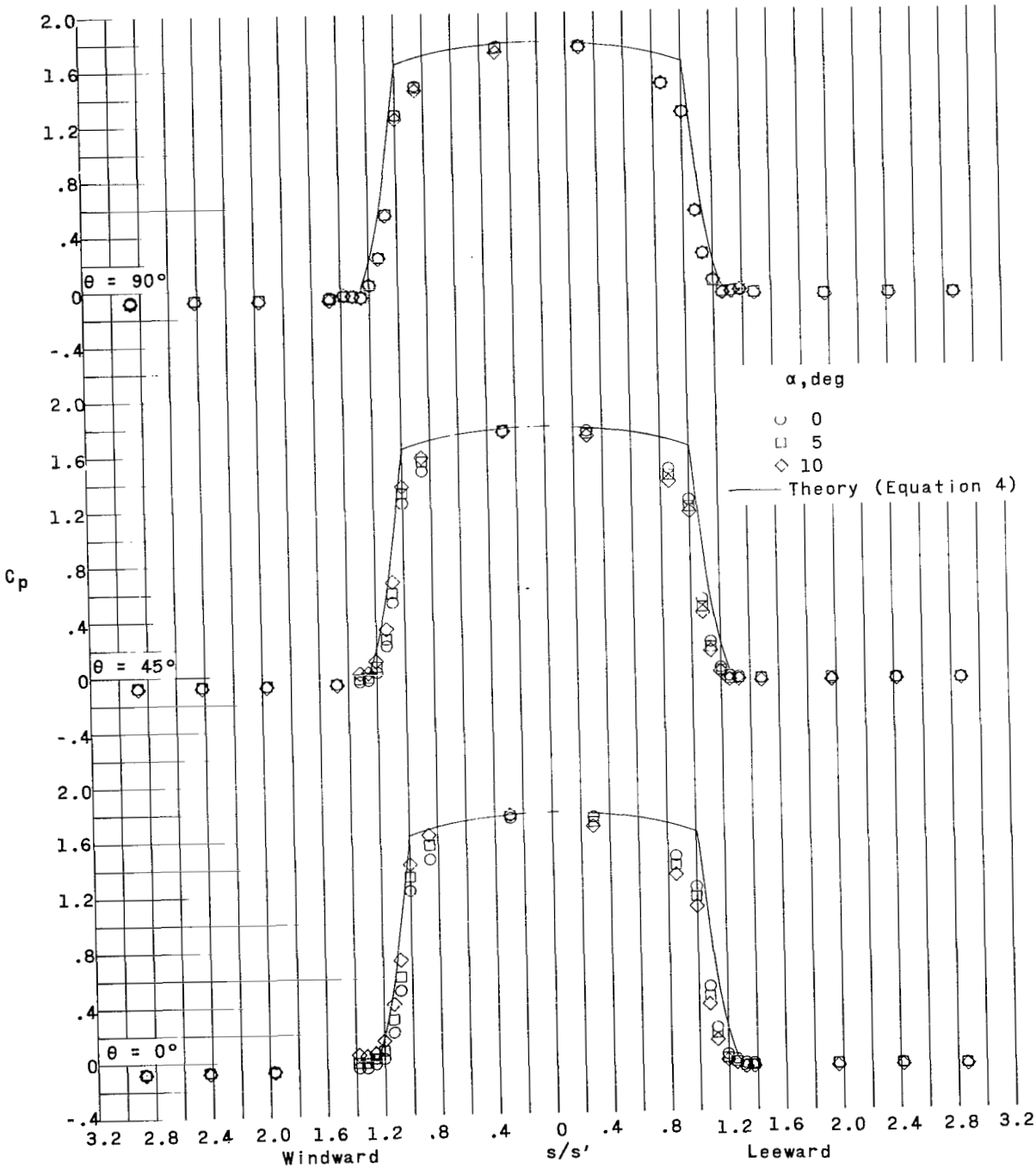

(a) Basic configuration.

Figure 4.- Effect of angle of attack on pressure distribution with and without probe protuberances installed on basic configuration; M = 3.51; R = 3.60×10^6.

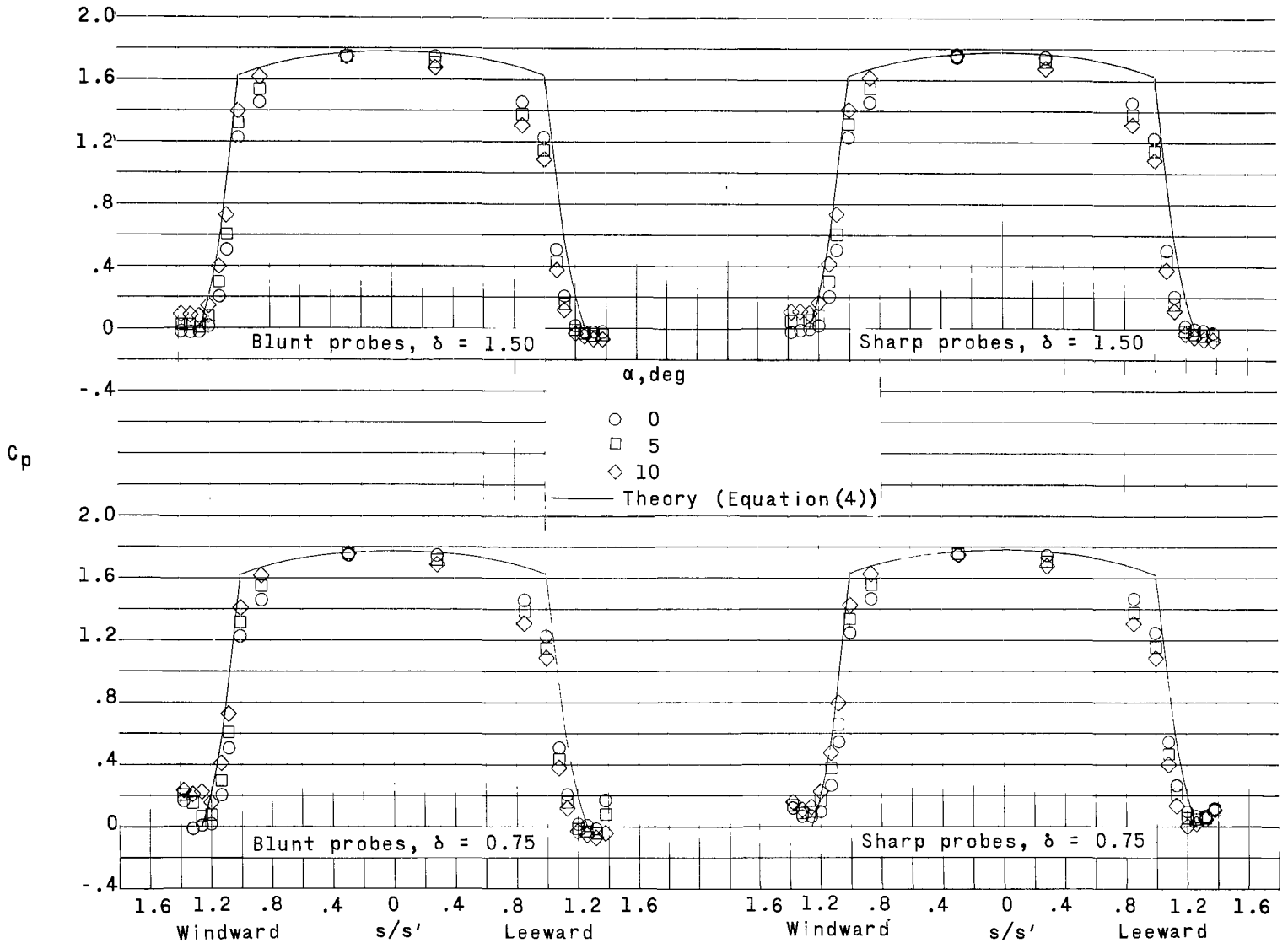

(b) Basic configuration with probes. $\theta = 0^{o}$.

Figure 4.- Concluded.

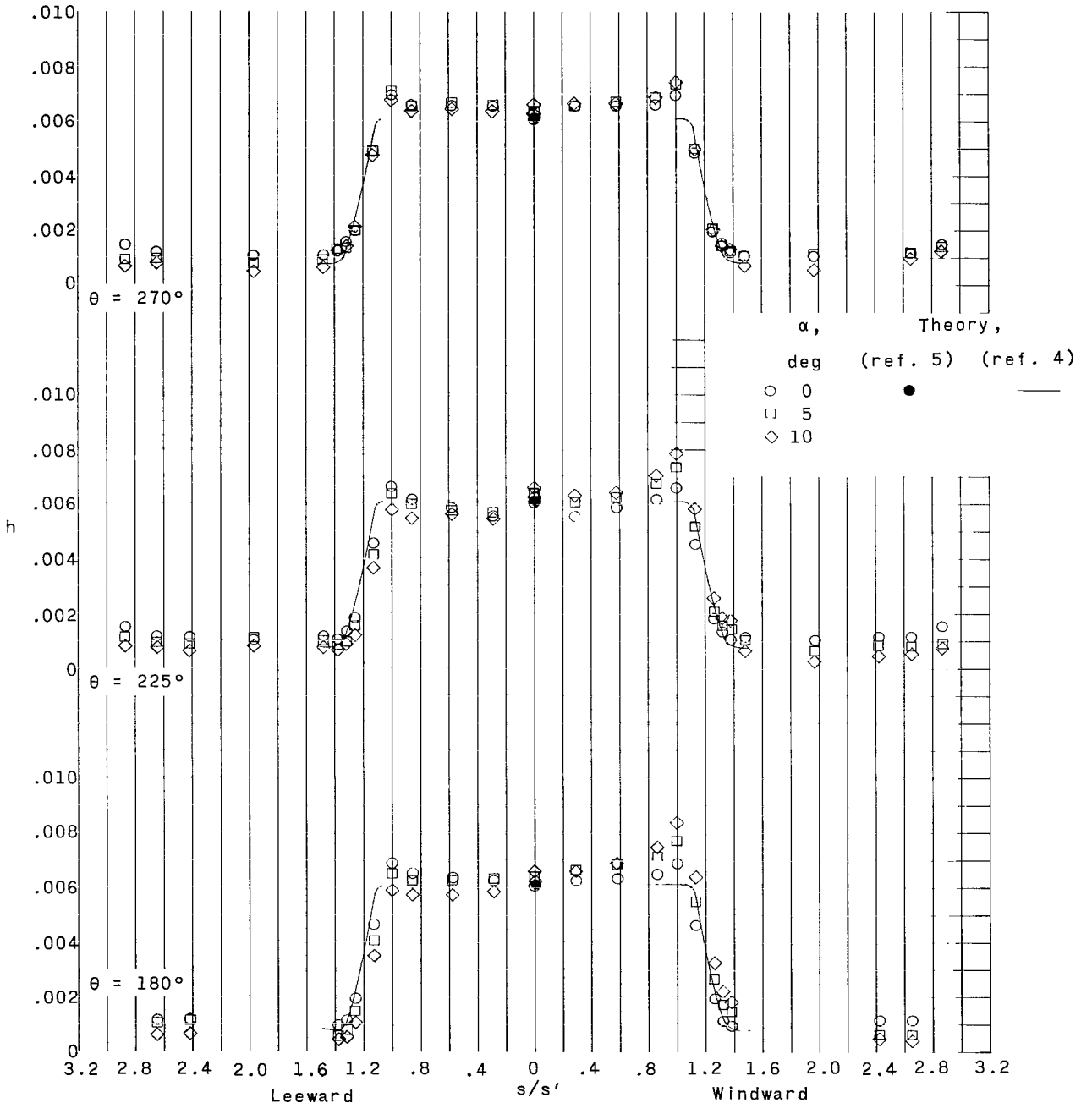

(a) Basic configuration.

Figure 5.- Effect of angle of attack on heat-transfer distribution with and without probe protuberances installed on basic configuration; M = 3.51; R = 3.60×10^6.

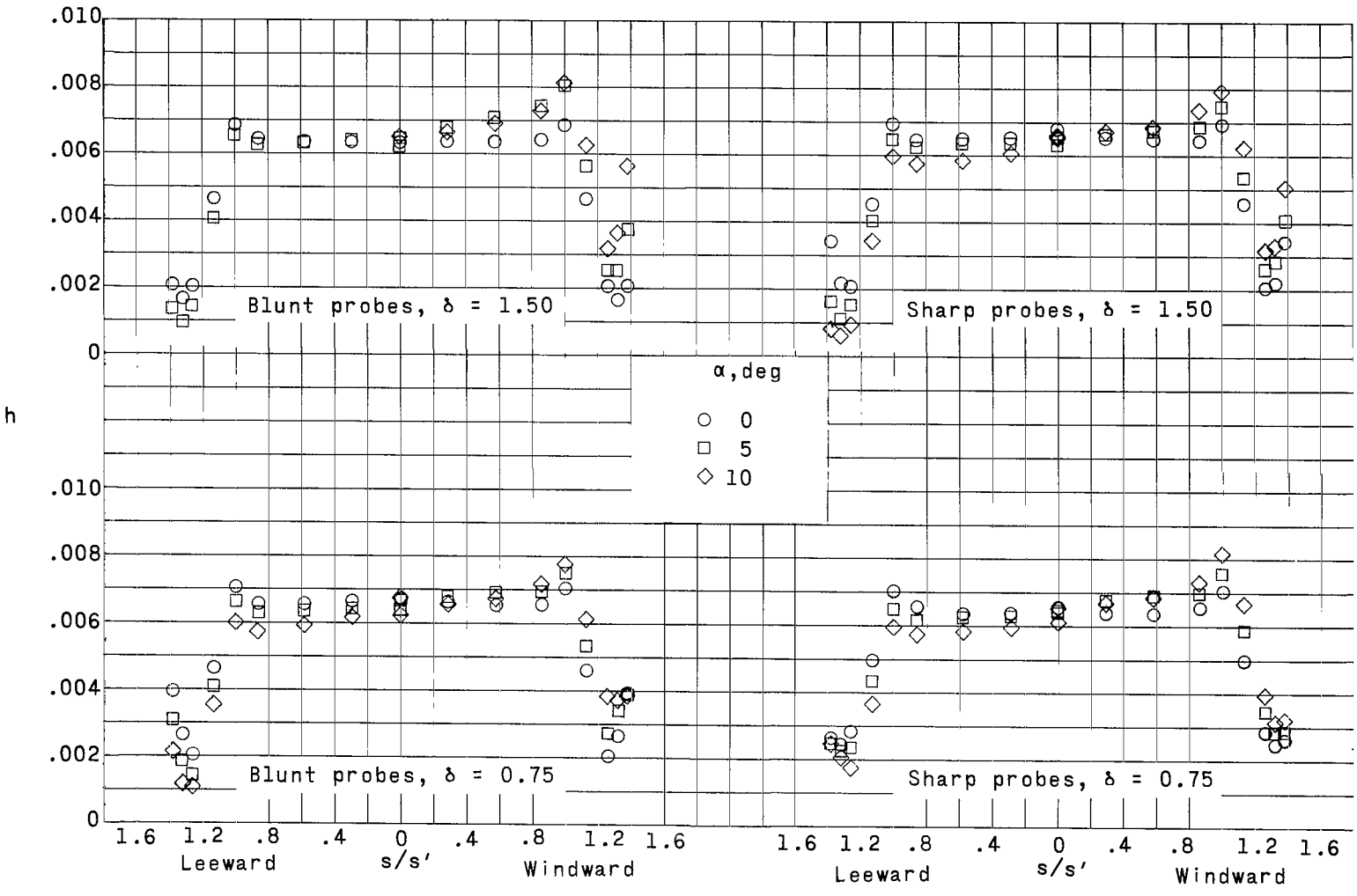

(b) Basic configuration with probes. $\theta = 180^{\circ}$.

Figure 5.- Concluded.

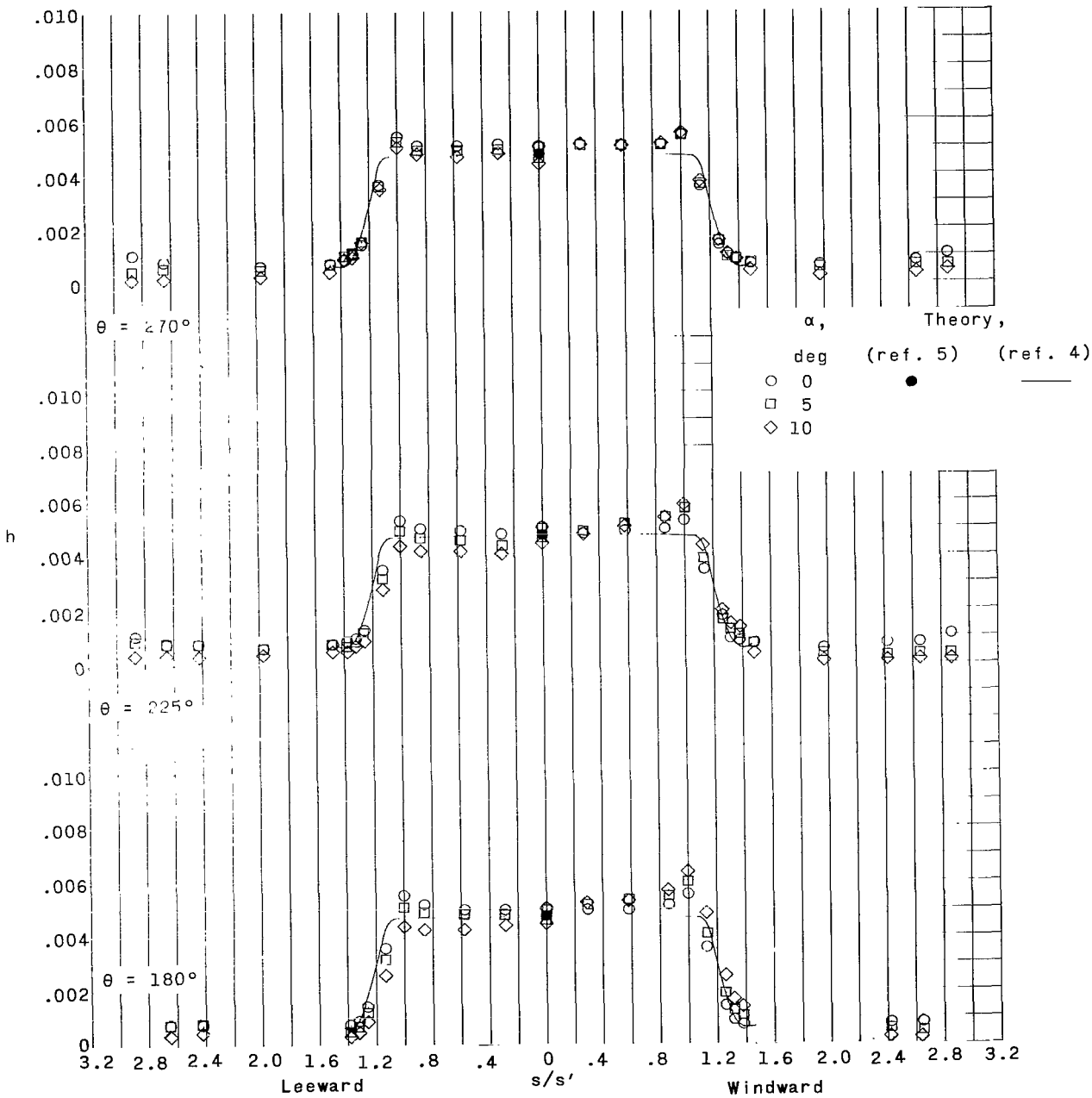

Figure 6.- Effect of angle of attack on heat transfer to basic configuration; $M = 3.51$; $R = 2.10 \times 10^6$.

"The aeronautical and space activities of the United States shall be conducted so as to contribute . . . to the expansion of human knowledge of phenomena in the atmosphere and space. The Administration shall provide for the widest practicable and appropriate dissemination of information concerning its activities and the results thereof."

—NATIONAL AERONAUTICS AND SPACE ACT OF 1958

NASA SCIENTIFIC AND TECHNICAL PUBLICATIONS

TECHNICAL REPORTS: Scientific and technical information considered important, complete, and a lasting contribution to existing knowledge.

TECHNICAL NOTES: Information less broad in scope but nevertheless of importance as a contribution to existing knowledge.

TECHNICAL MEMORANDUMS: Information receiving limited distribution because of preliminary data, security classification, or other reasons.

CONTRACTOR REPORTS: Technical information generated in connection with a NASA contract or grant and released under NASA auspices.

TECHNICAL TRANSLATIONS: Information published in a foreign language considered to merit NASA distribution in English.

TECHNICAL REPRINTS: Information derived from NASA activities and initially published in the form of journal articles.

SPECIAL PUBLICATIONS: Information derived from or of value to NASA activities but not necessarily reporting the results of individual NASA-programmed scientific efforts. Publications include conference proceedings, monographs, data compilations, handbooks, sourcebooks, and special bibliographies.

Details on the availability of these publications may be obtained from:

SCIENTIFIC AND TECHNICAL INFORMATION DIVISION

NATIONAL AERONAUTICS AND SPACE ADMINISTRATION

Washington, D.C. 20546